





Nonlinear enhancement of coherent magnetization dynamics

Mehrdad Elyasi ¹, Kei Yamamoto ², Tomosato Hioki,³ Takahiko Makiuchi ^{3,4},
Hiroki Shimizu,³ Eiji Saitoh,^{5,3,6,2} and Gerrit E. W. Bauer ^{5,7,8}

¹Advanced Institute for Materials Research, Tohoku University, Sendai 980-8577, Japan

²Advanced Science Research Center, Japan Atomic Energy Agency, Tokai 319-1195, Japan

³Department of Applied Physics, The University of Tokyo, Tokyo 113-8656, Japan

⁴Quantum-Phase Electronics Center, The University of Tokyo, Tokyo 113-8656, Japan

⁵WPI Advanced Institute for Materials Research, Tohoku University, Sendai 980-8577, Japan

⁶Institute for AI and Beyond, The University of Tokyo, Tokyo 113-8656, Japan

⁷Kavli Institute for Theoretical Sciences, University of the Chinese Academy of Sciences, Beijing 10090, China

⁸Zernike Institute for Advanced Materials, University of Groningen, 9747 AG Groningen, Netherlands



(Received 19 December 2023; revised 13 March 2024; accepted 15 April 2024; published 2 May 2024)

Magnets are interesting materials for classical and quantum information technologies. However, the short decoherence and dephasing times that determine the scale and speed of information networks severely limit the appeal of employing the ferromagnetic resonance. Here we show that the lifetime and coherence of the uniform Kittel mode can be enhanced by three-magnon interaction-induced mixing with the long-lived magnons at the minima of the dispersion relation. Analytical and numerical calculations based on this model explain recent experimental results and predict experimental signatures of quantum coherence.

DOI: [10.1103/PhysRevB.109.L180402](https://doi.org/10.1103/PhysRevB.109.L180402)

Introduction. Quantum information processing relies on the long coherence times of the elements in the network. These times can be enhanced by the controlled coupling of the information carrier to other long-lived degrees of freedom in hybrid devices [1]. For example, a collection of nitrogen-vacancy centers in diamond can act as a memory for cavity photons with lower quality [2–6]. Spin refocusing and dynamic decoupling of qubits from their environment are other schemes to tackle “black box dissipation/dephasing sources” [7,8].

The uniform magnetization oscillation or Kittel magnon strongly interacts with microwave photons and can be used to coherently control quantum states [9–13], and can be read out electrically [14]. However, its lifetime is often shorter than expected from the intrinsic Gilbert damping of yttrium iron garnet (YIG) with reported quality factors as large as 10^5 [15]. To realize, implement, and assess recent proposals for the generation of Kittel mode quantum states and their implementation in novel computational paradigms [11,16,17], the Kittel mode coherence must be pushed to its limits.

Magnon interactions have been mainly associated with an increase in dissipation or dephasing, which can be useful for the control of the magnon transport [18–21]. However, three-magnon interactions may also increase lifetimes. According to recent experiments, the Kittel mode lives longer by the coherent mixing with spin waves that have finite wave vectors [22–26]. We observed an excitation power-dependent enhanced lifetime of the Kittel mode or “persistent” coherence [26] and attributed it to three-magnon scattering (3MS). Similar physics also explains the power-dependent quenching of the magnon-photon interaction [27]. Here, we demonstrate how the valley magnons at the minima of the dispersion relation enhance the coherence lifetime of the Kittel mode in a monolithic magnet.

Model. Our generic model consists of three interacting bosonic modes $B_{1(2,3)}$ at (quasi-)equilibrium temperatures $T_{B_{1(2,3)}}$ and dissipation rates $\xi_{B_{1(2,3)}}$ with frequencies that satisfy $\omega_{B_1} = \omega_{B_2} + \omega_{B_3}$ and $\xi_{B_1} \gg \{\xi_{B_2}, \xi_{B_3}\}$ [see Fig. 1(a)]. We specialize in magnetic thin films with a sufficiently strong magnetodipolar coupling that generates a pronounced minimum frequency at finite wave vectors along the magnetization direction (valley magnons) [see Fig. 1(b)], such that B_1 is the $\vec{k} = 0$ Kittel mode with frequency ω_0 , and $B_{2(3)}$ is a valley magnon with momentum $+(-)\vec{k}_V$. The dispersion relations of magnetic disks agree with those of extended films of the same thickness as long as the demagnetizing fields are approximately constant across the sample and the frequency spacing of the standing waves does not exceed their inverse lifetime [28–30].

The magnetodipolar interaction becomes weaker with decreasing film thickness, with shallower valleys and a minimum frequency that exceeds $\sim \omega_0/2$, which suppresses the three-magnon scattering for YIG films with thickness $d \lesssim 800$ nm. However, in small disks, the inhomogeneous demagnetizing field at the edges pulls the frequencies below the valley minimum ω_{\min} with corresponding amplitudes localized at the edges. The 3MS interaction of these edge states with the Kittel magnons is therefore efficient even for thinner films [26].

The Lindblad master equation for the density matrix ρ of the driven interacting magnon gas reads [31–34]

$$\dot{\rho} = -i[\mathcal{H}^{(L)} + \mathcal{H}^{(NL)} + \mathcal{H}^{(d)}, \rho] + \sum_{\vec{k}} \xi_{\vec{k}} L_{\vec{k}}^{(L)}[\rho], \quad (1)$$

where $\vec{k} \in \{0, \vec{k}_V\}$. The system is tuned such that the valley magnon frequency is close to twice that of the Kittel mode, $\omega_{\vec{k}_V} \sim \omega_0/2$. In $\mathcal{H}^{(L)} = \sum_{\vec{k}} \Delta \omega_{\vec{k}} c_{\vec{k}}^\dagger c_{\vec{k}}$, $c_{\vec{k}}$ is the annihilation

operator of the \vec{k} magnon in a rotating frame so that $\Delta\omega_0 = 0$ and $\Delta\omega_{\vec{k}_v} = \omega_{\vec{k}_v} - \omega_0/2$. The leading magnon nonlinearities are $\mathcal{H}^{(NL)} = \mathcal{H}^{(3MS)} + \mathcal{H}^{(4MS)}$, where $\mathcal{H}^{(3MS)} = \sum_{\vec{k}_v} \mathcal{D}_{\vec{k}_v} c_0^\dagger c_{\vec{k}_v} c_{-\vec{k}_v} + \text{H.c.}$ is the three-magnon interaction with coefficient $\mathcal{D}_{\vec{k}_v}$, while $\mathcal{H}^{(4MS)}$ includes the four-magnon scattering terms [33,34]. Here we address the weak excitation regime in which we may disregard $\mathcal{H}^{(4MS)}$. The Kittel mode can be driven either resonantly or parametrically, i.e., $\mathcal{H}^{(d)} = (P_r c_0 + P_r^* c_0^\dagger) + (P_p c_0^2 + P_p^* c_0^{\dagger 2})$, with amplitudes P_r and P_p , respectively, that are proportional to the power of an external drive. $\xi_{\vec{k}}$ is a dissipation rate and $L_{\vec{k}}^{(L)}$ is a linear Lindblad dissipation operator that acts only in the Hilbert space of the \vec{k} mode,

$$L_{\vec{k}}^{(L)} = (\bar{n}_{\vec{k}} + 1)(2c_{\vec{k}}\rho c_{\vec{k}}^\dagger - c_{\vec{k}}^\dagger c_{\vec{k}}\rho - \rho c_{\vec{k}}^\dagger c_{\vec{k}}) + \bar{n}_{\vec{k}}(2c_{\vec{k}}^\dagger \rho c_{\vec{k}} - c_{\vec{k}}^\dagger c_{\vec{k}}\rho - \rho c_{\vec{k}}^\dagger c_{\vec{k}}), \quad (2)$$

and $\bar{n}_{\vec{k}}$ is the average particle number of a thermal bosonic bath formed by other magnons and/or phonons that at equilibrium, reduces to a Planck distribution at temperature T . Here we assume that a resonant microwave excitation drives the magnon dynamics. In experiments, a larger cone angle of the Kittel mode is efficiently excited by parametric pumping [26], but the associated magnetization dynamics is the same.

In the following, we address the lifetimes of the phase and amplitude of the coherent states of the Kittel mode as well as the quantum interferences of ‘‘Schrödinger cat states,’’ which are quantum superpositions of those coherent states.

Lifetime of coherent states. The effect of three-magnon scattering on classical coherence of the Kittel mode is at the hand of the mean-field amplitudes $\langle c_0 \rangle$ and $\langle c_{-\vec{k}_v} c_{\vec{k}_v} \rangle$, with a coupled equation of motion (EOM) that follows from the master Eq. (1),

$$\frac{d\langle c_0 \rangle}{dt} = -i \sum_{\vec{k}_v} \mathcal{D}_{\vec{k}_v} \langle c_{-\vec{k}_v} c_{\vec{k}_v} \rangle - \xi_0 \langle c_0 \rangle - iP_r^*, \quad (3)$$

$$\frac{d\langle c_{-\vec{k}_v} c_{\vec{k}_v} \rangle}{dt} = -i(2\Delta\omega_{\pm\vec{k}_v}) \langle c_{-\vec{k}_v} c_{\vec{k}_v} \rangle - i\mathcal{D}_{\vec{k}_v} [\langle c_0 \rangle (2\langle n_{\vec{k}_v} \rangle + 1)] - 2\xi_{\vec{k}_v} \langle c_{-\vec{k}_v} c_{\vec{k}_v} \rangle, \quad (4)$$

$$\frac{d\langle n_{\vec{k}_v} \rangle}{dt} = 2\mathcal{D}_{\vec{k}_v} \text{Im}[\langle c_0 \rangle \langle c_{-\vec{k}_v} c_{\vec{k}_v} \rangle] - 2\xi_{\vec{k}_v} (\langle n_{\vec{k}_v} \rangle - \bar{n}_{\vec{k}_v}), \quad (5)$$

where $n_{\vec{k}_v} = c_{\pm\vec{k}_v}^\dagger c_{\pm\vec{k}_v}$ [35].

We first consider a valley-magnon pair with a δ -function density of states at $\omega_0/2$, which is justified for relatively thin disks, as in Ref. [26]. We analyze the decay dynamics of a nonequilibrium state by switching off the external drive field and setting $\Delta\omega_{\pm\vec{k}_v} = 0$. For $t \ll 1/(2\xi_{\vec{k}_v})$, $\langle n_{\vec{k}_v} \rangle(t) \sim \langle n_{\vec{k}_v} \rangle(0)$ and Eq. (5) does not contribute. The solution is then $[\langle c_0 \rangle, \langle c_{\vec{k}_v} c_{-\vec{k}_v} \rangle]^T = A_+ e^{\lambda_+ t} v_+ + A_- e^{\lambda_- t} v_-$, where $\lambda_{\pm} = \frac{1}{2}[\pm\sqrt{\mathcal{A}} - \xi_0 - 2\xi_{\vec{k}_v}]$, $v_{\pm} = [-\xi_0 - 2\xi_{\vec{k}_v} \mp \sqrt{\mathcal{A}}, -2i\mathcal{D}_{\vec{k}_v} (2\langle n_{\vec{k}_v} \rangle + 1)]^T$, and $\mathcal{A} = (\xi_0 - 2\xi_{\vec{k}_v})^2 - 4\mathcal{D}_{\vec{k}_v}^2 (2\langle n_{\vec{k}_v} \rangle + 1)$. For $|4\mathcal{D}_{\vec{k}_v}^2 (\langle n_{\vec{k}_v} \rangle + 1)| \ll |(\xi_0 - 2\xi_{\vec{k}_v})^2|$, $\lambda_+ \approx -\xi_0$ and $\lambda_- \approx -2\xi_{\vec{k}_v}$, i.e., a fast (ξ_0) and slow ($2\xi_{\vec{k}_v}$) double exponential decay. When $4\mathcal{D}_{\vec{k}_v}^2 (2\langle n_{\vec{k}_v} \rangle + 1) > (\xi_0 - 2\xi_{\vec{k}_v})^2$, the Kittel mode amplitude oscillates with frequency

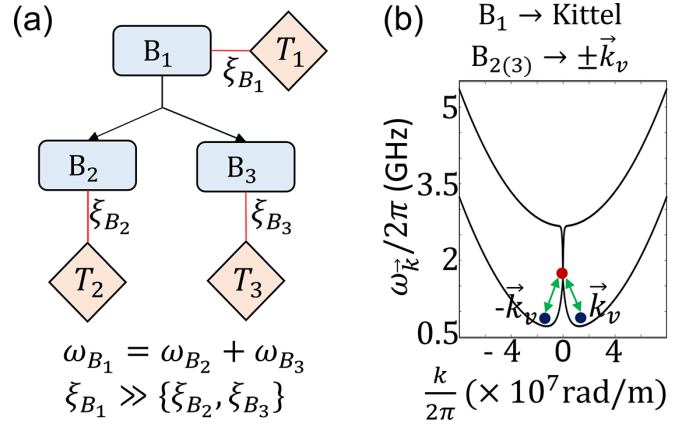


FIG. 1. (a) Schematics of the generic three-state model with frequencies ω and dissipation rates ξ . (b) In a thin film magnet, the Kittel mode interacts with valley magnon pairs with wave vectors $\pm\vec{k}_v$. Here we show the dispersion $\omega_{\vec{k}}$ of a $d = 1 \mu\text{m}$ YIG film, for $\vec{k} \parallel \vec{H}$ (bottom curve) and $\vec{k} \perp \vec{H}$ (top curve), where \vec{H} is an in-plane magnetic field.

$\sqrt{-\mathcal{A}}$ that is damped by $(\xi_0 + 2\xi_{\vec{k}_v})/2$. According to Eq. (5), $\langle n_{\vec{k}_v} \rangle$ decays such that after some time, $4\mathcal{D}_{\vec{k}_v}^2 (2\langle n_{\vec{k}_v} \rangle + 1) < (\xi_0 - 2\xi_{\vec{k}_v})^2$ may be the case, entailing a nonoscillatory decay $\sim 2\xi_{\vec{k}_v}$.

The hybridization of two bosons (e.g., magnons, photons, and phonons) with field operators a and b is often pursued based on the ‘‘beam-splitter’’ interaction $\mathcal{H}^{(BS)} = D(ab^\dagger + a^\dagger b)$, which becomes strong at resonances, e.g., in cavity magnonics [17] or standing sound waves in magnetic mechanical resonators [36]. The EOM of the Kittel mode c_0 and a boson b with dissipation rate $2\xi_{\vec{k}_v}$ is the same as Eqs. (3) and (4) when $\langle n_{\vec{k}_v} \rangle = 0$ and $\mathcal{D}_{\vec{k}_v} = D$. The differences between the nonlinear 3MS and the hybridized systems arise from the non-Hermitian self-consistent effective coupling that can be tuned via $\langle n_{\vec{k}_v} \rangle$, while D is a fixed parameter [22–25,37,38].

We show in the following that numerical solutions of Eq. (1) corroborate the simple picture sketched above. In Fig. 2(a), we show results for resonant excitation in the time interval $t \in [0, t_s]$ with $P_r \neq 0$. The decay of $\langle c_0 \rangle(t)$ with and without 3MS interaction ($\mathcal{D}_{\vec{k}_v} = 0$ and $\bar{n}_0 = \bar{n}_{\vec{k}_v} = 0$) is drastically different for $t > t_s$, changing from fast (ξ_0) to slow ($2\xi_{\vec{k}_v}$) even for a relatively weak $\mathcal{D}_{\vec{k}_v} \ll (\xi_0 - 2\xi_{\vec{k}_v})/2$, as predicted by the simple model. Figure 2(b) illustrates the effect of a relatively large 3MS interaction, while maintaining $2\mathcal{D}_{\vec{k}_v} < \xi_0 - 2\xi_{\vec{k}_v}$ for different thermal occupations of the valley magnons $\bar{n}_{\vec{k}_v}$ that can be tuned by parametric pumping, the 4MS, and magnon-conserving phonon scattering. When $\bar{n}_{\vec{k}_v} = 0$, $\langle n_{\vec{k}_v} \rangle(t_s)$ remains negligibly small and the dynamics is a fast decay followed by a slow one [black line in Fig. 2(b)]. When we increase the average occupation of valley magnons to $\bar{n}_{\vec{k}_v} = 3.5\Theta(t - t_s)$, where $\Theta(t - t_s)$ is the Heaviside function, the 3MS becomes strong. When $\mathcal{D}_{\vec{k}_v}^2 [2\langle n_{\vec{k}_v} \rangle(t) + 1] > (\xi_0 - 2\xi_{\vec{k}_v})^2$, the Rabi oscillation [red line in Fig. 2(b)] is damped by $(\xi_0 + 2\xi_{\vec{k}_v})/2$. Adopting $\bar{n}_{\vec{k}_v} = 3.5e^{-2\xi_{\vec{k}_v}(t-t_s)}\Theta(t - t_s)$, which decays by $2\xi_{\vec{k}_v}$, leads to the green line in Fig. 2(b) that initially decays like the strong coupling case, but then by $2\xi_{\vec{k}_v}$.

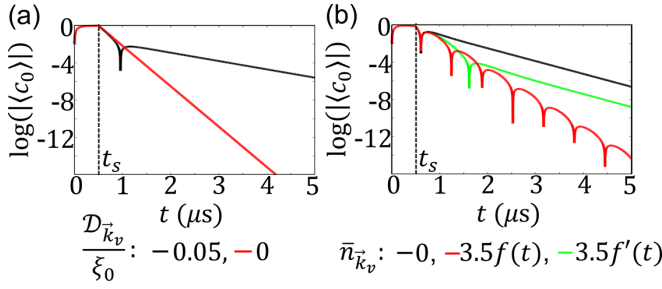


FIG. 2. Numerical calculation of the Kittel mode decay in the presence of a single valley magnon pair under resonant excitation $P_r = 0.5\xi_0[\Theta(t) - \Theta(t - t_s)]$, $\xi_0 = 1$ MHz, $\xi_{k_v} = 0.1$ MHz, $\mathcal{H}^{(AMS)} = 0$. (a) $\langle c_0 \rangle(t)$ for two values of $\mathcal{D}_{k_v}^-/\xi_0 = 0.05$ and 0 and zero temperature $\bar{n}_{0(k_v)} = 0$. (b) $\langle c_0 \rangle(t)$ for three different $\bar{n}_{k_v}^- = 0, 3.5f(t)$, and $3.5f'(t)$, where $f(t) = \Theta(t - t_s)$ and $f'(t) = \Theta(t - t_s) \exp[-2\xi_{k_v}(t - t_s)]$, for a stronger interaction $\mathcal{D}_{k_v}^-/\xi_0 = 0.25$. Here, and throughout the paper, log is in basis of 10.

Depending on the shape of the magnet and the applied magnetic field, the Kittel mode may interact with a quasicontinuum rather than a discrete state of valley magnons, such as in a relatively thick and wide film with $\omega_0/2 \geq \omega_{\min}$, as in Fig. 1(b). This scenario is similar to that of monochromatic photons interacting with an inhomogeneously broadened ensemble of NV center spins [2–6]. Here we introduce the frequency-dependent interaction parameter $\mathcal{G}(\omega)$ that governs the dynamics of the Kittel mode immersed into a continuum. We extend our theory by considering two limiting cases of

$$\mathcal{G}(\omega) = \mathcal{R}(\omega)\bar{\mathcal{D}}(\omega), \quad (6)$$

where $\mathcal{R}(\omega)$ is the density of states (DOS) of valley magnons, and $\bar{\mathcal{D}}(\omega)$ is the average of $\mathcal{D}_{k_v}^-$ at frequency ω ,

$$(I) \mathcal{G}^{(I)}(\omega) = C\Theta(\omega - \omega_0/2), \quad (II) \mathcal{G}^{(II)} = C, \quad (7)$$

where C is a constant. (I) and (II) correspond to $\omega_{\min} = \omega_0/2$ and $\omega_{\min} \ll \omega_0/2$, respectively. Figure 3(a) shows the calculated dynamics for $C = 0.1$, in which the decay for (I) is both fast (ξ_0) and slow ($2\xi_{k_v}^-$), while for (II) it is only fast. Next, we explain the dependence of the persistent coherence on the spectrum of valley magnons in more detail.

The dynamics at $t > t_s$ is easy to understand when the valley magnons are initially incoherent, i.e., $\langle c_{k_v}^+ c_{-k_v}^- \rangle|_{\omega_{k_v} = \omega}(t_s) = 0$. From the full numerical calculations with $\langle c_{k_v}^+ c_{-k_v}^- \rangle|_{\omega_{k_v} = \omega}(t_s) \neq 0$, we conclude that coherent valley magnons do not affect the time scales of interest. Equations (3)–(5) then lead to

$$\begin{aligned} \partial_t \langle c_0 \rangle(t) &= -\xi_0 \langle c_0 \rangle(t) - \int_0^\infty \mathcal{G}(\omega) [2\langle n_\omega \rangle + 1] d\omega \\ &\times \int_0^t d\tau e^{-i(2\Delta\omega - 2i\xi_{k_v}^-)(t-\tau)} \langle c_0 \rangle(\tau), \end{aligned} \quad (8)$$

for constant $\langle n_{k_v}^- \rangle|_{\omega_{k_v} = \omega} = \langle n_\omega \rangle(t) = \langle n_\omega \rangle(0)$. The solution of Eq. (8) [5] is

$$\langle c_0 \rangle(t) = \langle c_0 \rangle(0) \left[\sum_i R_i + Q \right], \quad (9)$$

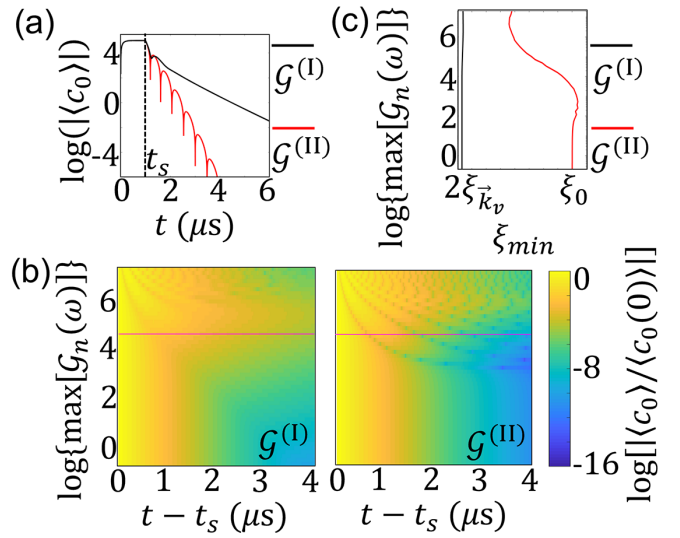


FIG. 3. Decay dynamics for a spectrum of valley magnons and dependence of frequency-dependent interaction parameter $\mathcal{G}(\omega)$. (a) The time evolution for $\mathcal{G}^{(I)} = 0.1\Theta(\omega - \omega_0/2)$ and $\mathcal{G}^{(II)} = 0.1$. $P_r/\xi_0 = 10^5$. (b) The dependence of $\langle c_0 \rangle(t)$ calculated from Eq. (9), on the peak amplitude of $\mathcal{G}_n(\omega)$, for $\mathcal{G}^{(I)}$ (left panel) and $\mathcal{G}^{(II)}$ (right panel). The magenta lines in (b) correspond to $\langle n_\omega \rangle(t_s)$ in (a). (c) The minimum decay rate ξ_{\min} calculated from the last 2 μs of the dynamics plotted in (b) at each $\max[\mathcal{G}_n(\omega)]$.

where

$$Q = e^{-2\xi_{k_v}^- t} \int_0^\infty \mathcal{G}_n(x/2) \mathcal{B}(x) e^{-ixt} dx, \quad (10)$$

$\mathcal{G}_n(x) = \mathcal{G}(x)[2\langle n_x \rangle + 1]$, R_i are the residues of $e^{st}\mathcal{L}$ at the poles s_i of $\mathcal{L} = \{s + \xi_0 + \int_0^\infty d\omega \mathcal{G}_n(\omega)[s + i(2\Delta\omega - 2i\xi_{k_v}^-)]^{-1}\}^{-1}$, $\mathcal{B}(x) = \{[\pi \mathcal{G}_n(x/2)/2]^2 + [i(\xi_0 - \xi_{k_v}^-) + x - \omega_0 + \mathcal{P}(x)/2]^2\}^{-1}$, and $\mathcal{P}(x)$ is the Cauchy principle value of $\int_0^\infty \mathcal{G}_n(\omega'/2) d\omega' / (\omega' - x)$.

Here, $\langle n_\omega \rangle$ at $t = t_s$ in Fig. 3(a) is best fit by a Gaussian of broadening $2\xi_{k_v}^-$. We determine $\langle c_0 \rangle(t)$ from Eq. (9) by evaluating the poles s_i and calculating the integral in Q , for $\mathcal{G}^{(I)}$ and $\mathcal{G}^{(II)}$. In Fig. 3(b), we assess the dependence of $\langle c_0 \rangle(t)$ on the peak amplitude of \mathcal{G}_n , which can be experimentally accessed by varying $\langle n_\omega(t_s) \rangle$. For $\mathcal{G}^{(I)}$ ($\mathcal{G}^{(II)}$), the decay rate of the tails of the dynamics is $\xi_{\min} \sim 2\xi_{k_v}^-$ ($\xi_{\min} \gg 2\xi_{k_v}^-$) [see Fig. 3(c)]. For $\mathcal{G}^{(I)}$, the two-exponential dynamics persists even in the strong coupling regime, while for $\mathcal{G}^{(II)}$, the decay rate remains $\gg 2\xi_{k_v}^-$ throughout, when increasing $\max[\mathcal{G}_n(\omega)]$ from relatively small to large values. We thus confirm that an asymmetry of $\mathcal{G}(\omega)$ with respect to and in the vicinity of $\omega_0/2$ is a necessary condition for reaching the limiting lifetime of $2\xi_{k_v}^-$, i.e., we should stay close to the band edge.

The difference between the dynamics associated with $\mathcal{G}^{(I)}$ and $\mathcal{G}^{(II)}$ can be illustrated by the spectrum $T(\omega_t) = \langle c_0 \rangle(\omega_t) / P_{r,t}$, which is the response to an excitation $P_r = P_{r,t} e^{-i\omega_t t}$, while $\langle c_0 \rangle(\omega_t)$ is the steady state of $\langle c_0 \rangle$ at frequency ω_t , and ω_t is in the frame of ω_0 . With $|P_{r,t}| = 1/\xi_0$, $T(\omega_t)$ follows from Eqs. (3) and (4) for constant $\langle n_{k_v}^- \rangle$. When $\mathcal{D}_{k_v}^- = 0$, $|T(0)| = 1$. When $\mathcal{D}_{k_v}^- \neq 0$ and $\lim_{2\xi_{k_v}^- \rightarrow 0} |T(\omega_t)| = 1$ for some ω_t , the Kittel

mode decays at the limiting rate of $2\xi_{k_v}$. Straightforward algebra leads to $\lim_{2\xi_{k_v} \rightarrow 0} T(\omega_t) = i\xi_0\{\omega_t + \mathcal{P}(\omega_0 + \omega_t)/2\} + i[\xi_0 + \pi\mathcal{G}_n[(\omega_0 + \omega_t)/2]/2]^{-1}$. In the case of $\mathcal{G}^{(I)}$, $\text{Im}[-iT(\omega_t)^{-1}] > 1\forall\omega_t$, thereby $|T(\omega_t)| < 1$. On the other hand, when $\omega_t < 0$ for $\mathcal{G}^{(II)}$, we have $\mathcal{G}_n[(\omega_t + \omega_0)/2] = 0$. Since $\lim_{\omega_t \rightarrow 0^-} \mathcal{P}(\omega_t + \omega_0)/2 = \infty$ and $\lim_{\omega_t \rightarrow -\infty} \mathcal{P}(\omega_t + \omega_0)/2 = 0$, $\omega_t + \mathcal{P}(\omega_t + \omega_0)/2 = 0$ for an $\omega_t < 0$ at which $T(\omega_t) = 1$ is reached. For the partially suppressed density of states in $\mathcal{G}^{(II)}$, we therefore predict effects that resemble those of spectral hole burning of inhomogeneously broadened NV center spin ensembles, an established method to reach the dissipation rate of individual spins [3,4].

Next, we address material dependence for samples of equal size. The 3MS coefficient $\mathcal{D}_{\vec{k}} = \omega_M \mathbf{g}_{\vec{k}} \sin \theta_{\vec{k}} \cos \theta_{\vec{k}} (u_{\vec{k}} + v_{\vec{k}}) (u_{\vec{k}} v_0 + v_{\vec{k}} u_0) / \sqrt{2S}$ [33], where $u_{\vec{k}} = \sqrt{(A_{\vec{k}} + \omega_{\vec{k}})/2\omega_{\vec{k}}}$ and $v_{\vec{k}} = -\text{sign}(B_{\vec{k}}) \sqrt{[(A_{\vec{k}} - \omega_{\vec{k}})/2\omega_{\vec{k}}]}$, $A_{\vec{k}} = \omega_H + \omega_M/2[2\alpha_{ex}k^2 + \mathbf{g}_{\vec{k}} \sin^2 \theta_{\vec{k}} + 1 - \mathbf{g}_{\vec{k}}]$, $B_{\vec{k}} = \omega_M/2[\mathbf{g}_{\vec{k}} \sin^2 \theta_{\vec{k}} + \mathbf{g}_{\vec{k}} - 1]$, $\mathbf{g}_{\vec{k}} = 1 - [1 - e^{-kd}]/kd$, $\alpha_{ex} = 2A_{ex}/\mu_0 M_s^2$, $\theta_{\vec{k}}$ is the in-plane angle of \vec{k} with magnetization, A_{ex} is the exchange stiffness, M_s is the saturation magnetization, $\omega_M = \mu_0 \gamma M_s$, $\omega_H = \mu_0 \gamma H$, and γ is the gyromagnetic ratio, $S = VM_s/(\hbar\gamma)$ is the number of spins, and V is the sample volume. Since for valley magnons $u_{\vec{k}} \sim 1$ and $v_{\vec{k}} \sim 0$, $\mathcal{D}_{\pm\vec{k}_v} \propto \sqrt{\omega_M}$.

From $\omega_{\vec{k}} = \sqrt{A_{\vec{k}}^2 - |B_{\vec{k}}|^2}$ and some simple algebra, we find the k_{\min} associated with ω_{\min} . The approximation $k_{\min} \approx 1/\sqrt{4d\alpha_{ex}}$ is justified for $\omega_H \gg \omega_M \alpha_{ex} k_{\min}^2$. $\omega_{\min}^2 \approx \omega_H^2 + 5\omega_M^2 \alpha_{ex} k_{\min}^2 / (4d) + \omega_M \omega_H [2\alpha_{ex} k_{\min}^2 + 1/(k_{\min} d)]$, while $\omega_0^2 = \omega_H^2 + \omega_M \omega_H$. A_{ex} increases while α_{ex} decreases with M_s . Therefore, ω_{\min} increases with M_s , but less so than ω_0 . Since the curvature $\partial^2 \omega_{\vec{k}} / \partial k^2|_{k=k_{\min}}$, and $\omega_{\vec{k}}^2 - \omega_{\min}^2 \approx \omega_H \omega_M \theta_{\vec{k}}^2$ when $|\vec{k}| = k_{\min}$, increase with M_s , the DOS of the valley magnons does not change much. For the given material parameters and sufficiently thick films, $\omega_{\min} = 2\omega_0$ can always be reached by applying a magnetic field. The interaction spectrum $\mathcal{G}(\omega)$ can therefore be tuned without changing the material simply by the sample thickness and the magnetic field.

In Fig. 4(a), we plot the frequency dependence of the DOS $\mathcal{R}(\omega)$, and average interaction strength $\bar{\mathcal{D}}(\omega)$ for a magnetic disk with thickness $d = 1 \mu\text{m}$ and radius $r = 100 \mu\text{m}$ for typical parameters of YIG and permalloy (Py). $\bar{\mathcal{D}}(\omega)$ vanishes at the band edge, but then increases rapidly with ω . M_s and A_{ex} of Py are almost 10 times larger than those of YIG. According to our analysis above, the DOS amplitude is about the same, but $\bar{\mathcal{D}}$ increases substantially. We solve Eqs. (3)–(5) for the $\mathcal{R}(\omega)$ and $\bar{\mathcal{D}}(\omega)$ of YIG for different values of $\Delta\omega' = \omega_0/2 - \omega_{\min}$, which can be tuned by the external field H [see Fig. 4(a)]. For better comparison, the drive is switched off at a time t_s at which $\max\langle n_{\omega} \rangle / S = 10^{-10}$, chosen to be small enough that 4MS interactions may be disregarded. Figures 4(b) and 4(c) show that the slow decay sets in faster and the coherence persists much longer when $\Delta\omega' \rightarrow 0$. The relatively small (large) detuning corresponds to the case $\mathcal{G}^{(I)}$ ($\mathcal{G}^{(II)}$). Since $\bar{\mathcal{D}}$ is larger for materials with larger M_s , such as Py, the persistent coherence of YIG can be achieved with weaker drive, but it requires a larger H . For sufficiently large lateral dimension $r > 10 \mu\text{m}$, $\mathcal{R}(\omega)$ of the valley magnons does not change with r , while $\bar{\mathcal{D}}(\omega) \propto 1/r$. So, smaller disks require weaker

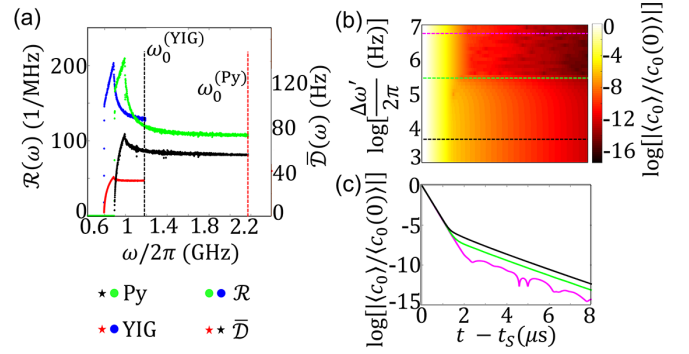


FIG. 4. Calculated results for a magnetic thin disk (thickness $d = 1 \mu\text{m}$, radius $100 \mu\text{m}$) at an external magnetic field $H = 25 \text{ mT}$. (a) Density of states $\mathcal{R}(\omega)$ and mean value of the 3MS interaction coefficient $\bar{\mathcal{D}}$ up to the FMR frequencies $\omega_0^{\text{YIG(Py)}}$. (b) The dependence of the decay $\log\langle c_0(t) \rangle$ on the detuning $\Delta\omega' = \omega_0/2 - \omega_{\min}$ for $P_r/\xi_0 = 10^5$. (c) Time evolution for three $\Delta\omega'$ [indicated by dashed lines colored as in (b)]. In calculations, we used the spectrum of 0.1 GHz width centered around $\omega_0/2$ and discretization of 0.01 MHz . The oscillations in the relatively large $\Delta\omega'$ are the artifact of limited bandwidth and discretization.

excitation for the same effect. Concluding, as long as $\xi_0 \gg \xi_{\vec{k}}$, which still has to be proven for Py, a substantial persistent coherence is easier to achieve for Py than YIG, in spite of the larger Gilbert damping of the former.

Lifetime of quantum interferences. Here we address the decay of the quantum interferences in a nonclassical state such as a superposition of two coherent states that may differ from that of coherent states and their statistical superpositions. We focus on the quantum coherence of an initial nonclassical superposition of a Kittel mode coherent state. We adopt the Schrödinger cat state of the isolated Kittel mode as the initial state, $|\psi_0(0)\rangle = |\psi_{0,\text{cat}}\rangle = \mathcal{N}(|\alpha_0\rangle + |\alpha'_0\rangle)$, where $|\alpha_0\rangle$ and $|\alpha'_0\rangle$ are two distinct coherent states with amplitudes α_0 and α'_0 , respectively, and \mathcal{N} is a normalization constant. For simplicity and without loss of generality, we set $\alpha'_0 = -\alpha_0$ and $\text{Im}[\alpha_0] = 0$. For a Kittel mode in the absence of 3MS interaction, the density matrix in the presence of a linear dissipation expressed by the $L_{\vec{k}}^{(L)}$ Lindblad operators in Eq. (1) can be exactly solved as $\rho(t) = \mathcal{N}^2\{|\alpha_0(t)\rangle\langle\alpha_0(t)| + |-\alpha_0(t)\rangle\langle-\alpha_0(t)| + [\mathcal{C}(t) |-\alpha_0\rangle\langle\alpha_0| + \text{H.c.}]\}$, where $\alpha(t) = \alpha_0 e^{-\xi_0 t}$. $\mathcal{C}(t) = e^{-2\xi_0 t} \exp[-4\alpha_0^2(1 - e^{-\xi_0 t})]$ [39,40] determines the difference between quantum and statistical superposition and vanishes faster than $|\alpha(t)|^2$. At long times, the state becomes a completely statistical rather than quantum superposition. Adding a resonant drive $P_r(c_0 + c_0^\dagger)$, $\alpha(t) = \alpha_0 e^{-\xi_0 t} + (iP_r/\xi_0)(e^{-\xi_0 t} - 1)$ does not affect $\mathcal{C}(t)$.

We now assess the effect of 3MS on the density matrix in the Hilbert space of the Kittel mode and a pair of valley magnons for two distinct initial conditions $\rho_{\text{cat}}(0) = |\psi_{0,\text{cat}}\rangle\langle\psi_{0,\text{cat}}| \otimes \rho_{\pm\vec{k}_v,\text{vac}}$ and $\rho_{\text{stat}}(0) = |\psi_{0,\text{stat}}\rangle\langle\psi_{0,\text{stat}}| \otimes \rho_{\pm\vec{k}_v,\text{vac}}$, where “vac” indicates valley magnon vacuum, $|\psi_{0,\text{stat}}\rangle\langle\psi_{0,\text{stat}}| = \mathcal{N}'(|\alpha_0\rangle\langle\alpha_0| + |-\alpha_0\rangle\langle-\alpha_0|)$ is a statistical mixture of two coherent states, and \mathcal{N}' is a normalizing constant. We label the density matrices evolving from these two initial conditions, $\rho_{\text{cat}}(t)$ and $\rho_{\text{stat}}(t)$, and integrate the valley magnons out to obtain an effective density matrix of

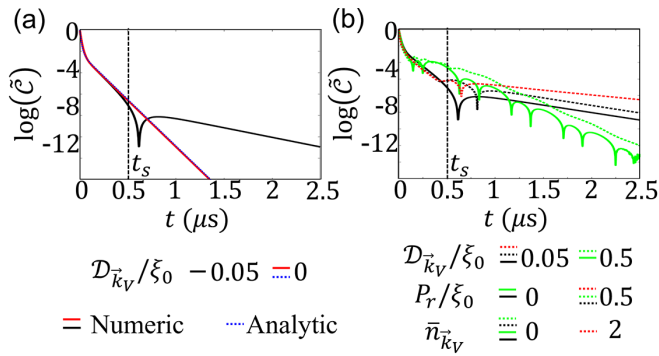


FIG. 5. Decay of quantum coherence. (a) $\tilde{C}(t)$ as a function of time with relatively weak and completely without 3MS interactions. The blue dashed line is our analytical result in the presence of 3MS. (b) $\tilde{C}(t)$ with and without the resonant drive of the Kittel mode, now for weak and strong 3MS interactions. The red dashed line holds for $\bar{n}_{\bar{k}_v} = 2$ for weak 3MS and $P_r \neq 0$.

the Kittel mode, $\rho_{0,\text{cat}(\text{stat})}$. For a measurement operator \hat{O} with eigenvalues o and eigenstates $|\phi\rangle$, the coherence of an arbitrary state $|\psi\rangle = \sum_i c_i |\phi_i\rangle$, where $c_i = \langle\psi|\phi_i\rangle$, emerges in the probability distribution $P(o)$ as $\sum_{i \neq j} \langle o|\phi_i\rangle \langle\phi_j|o\rangle$, which vanishes when \hat{O} is diagonal in $|\phi_i\rangle$. In other words, the quantum interferences become observables for a measurement operator that does not commute with the projection operator of the measured states [39]. Here the number operator serves this purpose via $p_{n,\text{cat}(\text{stat})} = \langle n|\rho_{0,\text{cat}(\text{stat})}(t)|n\rangle$, where $|n\rangle$ is the n number (Fock) state of the Kittel mode such that the time dependence of $\tilde{C}(t) = \sum_n [p_{n,\text{cat}} - p_{n,\text{stat}}] \neq C(t)$ measures the decay of the quantum coherence [39]. In the calculations below, we use the same dissipation parameters as before.

Figure 5(a) shows our results for $\tilde{C}(t)$ with and without (weak) 3MS and without drive $P_r = 0$, compared with the $C(t)$ (blue dashed line) for equal starting amplitudes $C(0) = \tilde{C}(0)$. We find that 3MS also increases the quantum coherence, similar to the effect of the beam-splitter interaction of hybrid systems. As discussed above, 3MS introduces a $\langle n_{\bar{k}_v} \rangle$

dependence; however, that may be indirectly tuned by driving the Kittel mode or directly occupying the valley magnons $\bar{n}_{\bar{k}_v}$. Figure 5(b) shows $\tilde{C}(t)$ when $P_r = 0$ and $P_r = 0.5\xi_0$, for a weak $\mathcal{D}_{\bar{k}_v}/\xi_0 = 0.05$ and a strong $\mathcal{D}_{\bar{k}_v}/\xi_0 = 0.5$ 3MS. The enhanced quantum coherence is evident. In Fig. 5(b), we demonstrate that the persistent coherence may be further enhanced when both $P_r = 0.5\xi_0$ and $\bar{n}_{\bar{k}_v} = 2$. The decay of the quantum coherence $\tilde{C}(t)$ limits the visibility of the negativity of the Wigner function of the Kittel mode in the tomography [14,26] at low temperatures, but, according to our calculations, the difference with the classical decay rates is minor.

Conclusion. We refine the model calculations of the interaction of the Kittel mode with valley magnons that enhances the magnetic coherence in extended films and microstructures. In spite of the rather weak nonlinear interactions in the samples and microwave powers explored to date, a substantial persistent coherence has been reported [26]. We uncover the role of the spectral dependence of three-magnon interactions, density of states, and applied magnetic fields, and predict that the decay rates of quantum and classical coherence are of the same order of magnitude. Our model also holds for materials such as Py and for other interacting three-level systems with mode-dependent dissipation rates [41], such as heterostructures composed of different magnetic materials [42] or nitrogen-vacancy centers in diamond [43]. Other interesting platforms are antiferromagnets such as MnF_2 with hyperfine interactions that generate Suhl-Nakamura-de Gennes nuclear spin waves [44–47]. The three-field resonance of electron spin waves, nuclei spin waves, and phonons was experimentally demonstrated long ago [48,49] and can now be modeled in a modern fashion and implemented for enhancing the lifetime of electron magnons.

Acknowledgments. We acknowledge support by JSPS KAKENHI (Grants No. 19H05600, No. 19H00645, No. 21K13847, No. 21K13886, No. 22H04965, No. 22K14584), JST CREST (Grant No. JPMJCR20C1), JST PRESTO (Grant No. JPMJPR20LB), Advanced Technology Institute Research Grants 2022, and partial support by the Institute for AI and Beyond of the University of Tokyo, and the IBM-UTokyo Laboratory.

- [1] Z.-L. Xiang, S. Ashhab, J. Q. You, and F. Nori, Hybrid quantum circuits: Superconducting circuits interacting with other quantum systems, *Rev. Mod. Phys.* **85**, 623 (2013).
- [2] S. Putz, D. O. Krimer, R. Amsüss, A. Valookaran, T. Nöbauer, J. Schmiedmayer, S. Rotter, and J. Majer, Protecting a spin ensemble against decoherence in the strong-coupling regime of cavity QED, *Nat. Phys.* **10**, 720 (2014).
- [3] S. Putz, A. Angerer, D. O. Krimer, R. Glattauer, W. J. Munro, S. Rotter, J. Schmiedmayer, and J. Majer, Spectral hole burning and its application in microwave photonics, *Nat. Photon.* **11**, 36 (2017).
- [4] D. O. Krimer, B. Hartl, and S. Rotter, Hybrid quantum systems with collectively coupled spin states: Suppression of decoherence through spectral hole burning, *Phys. Rev. Lett.* **115**, 033601 (2015).
- [5] D. O. Krimer, S. Putz, J. Majer, and S. Rotter, Non-Markovian dynamics of a single-mode cavity strongly coupled to an inhomogeneously broadened spin ensemble, *Phys. Rev. A* **90**, 043852 (2014).
- [6] B. Julsgaard, C. Grezes, P. Bertet, and K. Mølmer, Quantum memory for microwave photons in an inhomogeneously broadened spin ensemble, *Phys. Rev. Lett.* **110**, 250503 (2013).
- [7] L. Viola and S. Lloyd, Dynamical suppression of decoherence in two-state quantum systems, *Phys. Rev. A* **58**, 2733 (1998).
- [8] G. de Lange, Z. H. Wang, D. Riste, V. V. Dobrovitski, and R. Hanson, Universal dynamical decoupling of a single solid-state spin from a spin bath, *Science* **330**, 60 (2010).
- [9] D. Lachance-Quirion, S. P. Wolski, Y. Tabuchi, S. Kono, K. Usami, and Y. Nakamura, Entanglement-based single-shot detection of a single magnon with a superconducting qubit, *Science* **367**, 425 (2020).

- [10] M. Elyasi, Y. M. Blanter, and G. E. W. Bauer, Resources of nonlinear cavity magnonics for quantum information, *Phys. Rev. B* **101**, 054402 (2020).
- [11] H. Yuan, Y. Cao, A. Kamra, R. A. Duine, and P. Yan, Quantum magnonics: When magnon spintronics meets quantum information science, *Phys. Rep.* **965**, 1 (2022).
- [12] S. Sharma, V. A. S. V. Bittencourt, A. D. Karenowska, and S. V. Kusminskiy, Spin cat states in ferromagnetic insulators, *Phys. Rev. B* **103**, L100403 (2021).
- [13] M. Kounalakis, G. E. W. Bauer, and Y. M. Blanter, Analog quantum control of magnonic cat states on a chip by a superconducting qubit, *Phys. Rev. Lett.* **129**, 037205 (2022).
- [14] T. Hioki, H. Shimizu, T. Makiuchi, and E. Saitoh, State tomography for magnetization dynamics, *Phys. Rev. B* **104**, L100419 (2021).
- [15] D. D. Stancil and A. Prabhakar, *Spin Waves* (Springer, New York, 2009).
- [16] A. Chumak *et al.*, Advances in magnetics roadmap on spin-wave computing, *IEEE Trans. Magn.* **58**, 1 (2022).
- [17] B. Z. Rameshti, S. V. Kusminskiy, J. A. Haigh, K. Usami, D. Lachance-Quirion, Y. Nakamura, C.-M. Hu, H. X. Tang, G. E. W. Bauer, and Y. M. Blanter, Cavity magnonics, *Phys. Rep.* **979**, 1 (2022).
- [18] H. Kurebayashi, O. Dzyapko, V. E. Demidov, D. Fang, A. J. Ferguson, and S. O. Demokritov, Controlled enhancement of spin-current emission by three-magnon splitting, *Nat. Mater.* **10**, 660 (2011).
- [19] I. Barsukov, H. K. Lee, A. A. Jara, Y.-J. Chen, A. M. Goncalves, C. Sha, J. A. Katine, R. E. Arisa, B. A. Ivanov, and I. N. Krivorotov, Giant nonlinear damping in nanoscale ferromagnets, *Sci. Adv.* **5**, eaav6943 (2019).
- [20] B. Divinskiy, S. Urazhdin, S. O. Demokritov, and V. E. Demidov, Controlled nonlinear magnetic damping in spin-Hall nano-devices, *Nat. Commun.* **10**, 5211 (2019).
- [21] M. Mohseni, Q. Wang, B. Heinz, M. Kewenig, M. Schneider, F. Kohl, B. Lagel, C. Dubs, A. V. Chumak, and P. Pirro, Controlling the nonlinear relaxation of quantized propagating magnons in nanodevices, *Phys. Rev. Lett.* **126**, 097202 (2021).
- [22] V. E. Demidov, O. Dzyapko, S. O. Demokritov, G. A. Melkov, and A. N. Slavin, Thermalization of a parametrically driven magnon gas leading to Bose-Einstein condensation, *Phys. Rev. Lett.* **99**, 037205 (2007).
- [23] V. E. Demidov, O. Dzyapko, S. O. Demokritov, G. A. Melkov, and A. N. Slavin, Observation of spontaneous coherence in Bose-Einstein condensate of magnons, *Phys. Rev. Lett.* **100**, 047205 (2008).
- [24] A. A. Serga, V. S. Tiberkevich, C. W. Sandweg, V. I. Vasyuchka, D. A. Bozhko, A. V. Chumak, T. Neumann, B. Obry, G. A. Melkov, A. N. Slavin, and B. Hillebrands, Bose-Einstein condensation in an ultra-hot gas of pumped magnons, *Nat. Commun.* **5**, 3452 (2013).
- [25] D. A. Bozhko, A. A. Serga, P. Clausen, V. I. Vasyuchka, F. Heussner, G. A. Melkov, A. Pomyalov, V. S. Lvov, and B. Hillebrands, Supercurrent in a room-temperature Bose-Einstein magnon condensate, *Nat. Phys.* **12**, 1057 (2016).
- [26] T. Makiuchi, T. Hioki, H. Shimizu, K. Hoshi, M. Elyasi, K. Yamamoto, N. Yokoi, A. Serga, B. Hillebrands, G. E. W. Bauer, and E. Saitoh, Persistent magnetic coherence in magnets, *Nat. Mater.* (2024), doi: [10.1038/s41563-024-01798-z](https://doi.org/10.1038/s41563-024-01798-z).
- [27] O. Lee, K. Yamamoto, M. Umeda, C. W. Zollitsch, M. Elyasi, T. Kikkawa, E. Saitoh, G. E. W. Bauer, and H. Kurebayashi, Nonlinear magnon polaritons, *Phys. Rev. Lett.* **130**, 046703 (2023).
- [28] B. A. Kalinikos and A. N. Slavin, Theory of dipole-exchange spin wave spectrum for ferromagnetic films with mixed exchange boundary conditions, *J. Phys. C: Solid State Phys.* **19**, 7013 (1986).
- [29] B. A. Kalinikos, M. P. Kostylev, N. V. Kozhus, and A. N. Slavin, The dipole-exchange spin wave spectrum for anisotropic ferromagnetic films with mixed exchange boundary conditions, *J. Phys.: Condens. Matter* **2**, 9861 (1990).
- [30] M. J. Hurben and C. E. Patton, Theory of magnetostatic waves for in-plane magnetized isotropic films, *J. Magn. Magn. Mater.* **139**, 263 (1995).
- [31] H. J. Carmichael, *Statistical Methods in Quantum Optics 1* (Springer, New York, 1999).
- [32] H. J. Carmichael, *Statistical Methods in Quantum Optics 2* (Springer-Verlag, Berlin, 2008).
- [33] P. Krivosik and C. E. Patton, Hamiltonian formulation of nonlinear spin-wave dynamics: Theory and applications, *Phys. Rev. B* **82**, 184428 (2010).
- [34] M. Elyasi, E. Saitoh, and G. E. W. Bauer, Stochasticity of the magnon parametron, *Phys. Rev. B* **105**, 054403 (2022).
- [35] V. S. Lvov, *Wave Turbulence Under Parametric Excitation* (Springer-Verlag, Berlin, 1994).
- [36] K. An, R. Kohno, A. N. Litvinenko, R. L. Seeger, V. V. Naletov, L. Vila, G. de Loubens, J. Ben Youssef, N. Vukadinovic, G. E. W. Bauer, A. N. Slavin, V. S. Tiberkevich, and O. Klein, Bright and dark states of two distant macrospins strongly coupled by phonons, *Phys. Rev. X* **12**, 011060 (2022).
- [37] S. M. Rezende, Theory of coherence in Bose-Einstein condensation phenomena in a microwave-driven interacting magnon gas, *Phys. Rev. B* **79**, 174411 (2009).
- [38] A. Rückriegel and P. Kopietz, Rayleigh-Jeans condensation of pumped magnons in thin-film ferromagnets, *Phys. Rev. Lett.* **115**, 157203 (2015).
- [39] D. F. Walls and G. J. Milburn, *Quantum Optics* (Springer-Verlag, Berlin, 2008).
- [40] H. M. Wiseman and G. J. Milburn, *Quantum Measurement and Control* (Cambridge University Press, Cambridge, 2010).
- [41] L. Körber, K. Schultheiss, T. Hula, R. Verba, J. Fassbender, A. Kakay, and H. Schultheiss, Nonlocal stimulation of three-magnon splitting in a magnetic vortex, *Phys. Rev. Lett.* **125**, 207203 (2020).
- [42] L. Sheng, M. Elyasi, J. Chen, W. He, Y. Wang, H. Wang, H. Feng, Y. Zhang, I. Medlej, S. Liu, W. Jiang, X. Han, D. Yu, J.-P. Ansermet, G. E. W. Bauer, and H. Yu, Nonlocal detection of interlayer three-magnon coupling, *Phys. Rev. Lett.* **130**, 046701 (2023).
- [43] J. J. Carmiggelt, I. Bertelli, R. W. Mulder, A. Teepe, M. Elyasi, B. G. Simon, G. E. W. Bauer, Y. M. Blanter, and T. van der Sar, Broadband microwave detection using electron spins in a hybrid diamond-magnet sensor chip, *Nat. Commun.* **14**, 490 (2023).
- [44] H. Suhl, Effective nuclear spin interactions in ferromagnets, *Phys. Rev.* **109**, 606 (1958).
- [45] T. Nakamura, Indirect coupling of nuclear spins in anti-ferromagnet with particular reference to MnF_2 at very low temperatures, *Prog. Theor. Phys.* **20**, 542 (1958).

- [46] P. G. de Gennes, P. A. Pincus, F. Hartmann-Boutron, and J. M. Winter, Nuclear magnetic resonance modes in magnetic material. I. Theory, *Phys. Rev.* **129**, 1105 (1963).
- [47] Y. Shiomi, J. Lustikova, S. Watanabe, D. Hirobe, S. Takahashi, and E. Saitoh, Spin pumping from nuclear spin waves, *Nat. Phys.* **15**, 22 (2019).
- [48] A. V. Andrienko, V. I. Ozhogin, V. L. Safonov, and A. Yu. Yakubovskii, Nuclear spin wave research, *Sov. Phys. Usp.* **34**, 843 (1991).
- [49] L. W. Hinderks and P. M. Richards, Excitation of nuclear and electronic spin waves in RbMnF_3 by parallel pumping, *J. Appl. Phys.* **39**, 824 (1968).